PHYSICAL REVIEW B **80**, 174414 (2009)

Magnetic and electronic properties of $Eu_{1-x}Sr_xMnO_3$ ($0.3<x<0.7$) single crystals

Y. Tomioka,[1] R. Kumai,[2] T. Ito,[1] and Y. Tokura[3,4]
[1]*Nanoelectronics Research Institute (NeRI), National Institute of Advanced Industrial Science and Technology (AIST), Tsukuba 305-8562, Japan*
[2]*Photonics Research Institute, National Institute of Advanced Industrial Science and Technology (AIST), Tsukuba 305-8562, Japan*
[3]*Department of Applied Physics, University of Tokyo, Hongo, Bunkyo-ku, Tokyo 113-8656, Japan*
[4]*Cross-Correlated Materials Research Group (CMRG), Advanced Science Institute (ASI), RIKEN, 2-1 Hirosawa, Wako, Saitama 351-0198, Japan*

(Received 7 September 2009; revised manuscript received 20 October 2009; published 17 November 2009)

Among versatile perovskite manganites showing colossal magnetoresistance (CMR), $Eu_{1-x}Sr_xMnO_3$ around $x\sim0.4$ shows the ferromagnetic metal with the lowest transition temperature (~40 K) due to the narrowest one-electron bandwidth and hence is readily subject to the drastic phase changes with variations in temperature, magnetic field, and hole doping (x). We have investigated the variation in the electronic state with x with use of single crystals. As x increases, the ferromagnetic metal at $0.38\leq x\leq0.47$ changes to a spin-glasslike insulator at $0.48\leq x\leq0.5$, the layered antiferromagnetic (A-type) state at $0.51\leq x<0.6$, and the chained antiferromagnetic (C-type) state at $0.6\leq x$, respectively. Due to the increased disorder upon alloying of Eu/Sr, the charge/orbital ordering with the modulation vector (0, q, 0) with $q=1/2$ in the orthorhombic *Pbnm* setting ($a_0\sim b_0\sim c_0/\sqrt{2}\sim\sqrt{2}a_p$, a_p being the lattice parameter of the pseudocubic lattice) cannot be formed in a long range but remains short ranged. In the vicinity of $x=0.5$, an application of an external magnetic field removes such short-range charge/orbital ordering ($q=1/2$) to cause an insulator to metal transition or CMR. In a broad range of x ($0.55\leq x\leq0.59$), the critical temperature for the layered antiferromagnetic state is relatively lowered and alternatively the charge/orbital ordering with $q\sim1/3$ becomes to be visible. It has also been found that the modulation is temperature dependent; commensurate with $q\sim1/3$ upon the transition while incommensurate with $q>1/3$ at low temperatures.

DOI: 10.1103/PhysRevB.80.174414 PACS number(s): 71.27.+a, 71.30.+h, 75.30.Kz

I. INTRODUCTION

In the manganese oxides with perovskite structure, competing features are seen among several electronic phases with coupling among spin, charge, and orbital (lattice) degrees of freedom.[1–3] A fundamental property in the manganites is the metallic ferromagnetism due to the double exchange interaction[4–8] scaled by the effective one-electron bandwidth of the e_g-band (W).[9] The magnitude of W is tuned by a crystal lattice distortion in terms of the averaged radius of the perovskite A-site cations.[10] In $RE_{1-x}Sr_xMnO_3$ (RE being rare-earth elements) with $x\sim0.5$, the ferromagnetic metal (FM) is stabilized for $RE=$La (Refs. 11 and 12), but it is replaced with the charge/orbital ordering (the ordering of Mn^{3+}/Mn^{4+} with 1/1 accompanied by e_g-orbital ordering, CO/OO) for $RE=$Nd and Sm with the narrower W.[13,14] The modulation vector of the CO/OO at $x\sim1/2$ is expressed as (0, q, 0) with $q=1/2$ in the orthorhombic *Pbnm* setting ($a_0\sim b_0\sim c_0/\sqrt{2}\sim\sqrt{2}a_p$, where a_p is the lattice parameter of the pseudocubic lattice).[15]

In the manganites, an effect of quenched disorder on the phase competition is also of importance, the magnitude of which is quantified by the variance of the ionic radii of RE/AE (AE being alkaline-earth elements).[16–18] For a distorted manganite with larger quenched disorder, e.g., $Gd_{1-x}Sr_xMnO_3$ ($x\sim0.5$), a FM is not realized due to a narrowed W but the CO/OO ($q=1/2$) in a long range is also disrupted by increased disorder, which results in the ground state of a spin-glasslike insulator (SGI).[19] In $Eu_{1-x}Sr_xMnO_3$, similarly to $Gd_{1-x}Sr_xMnO_3$, a SGI is seen at $x\sim0.4$,[20,21] as earlier works have indicated.[20–25]

In this paper, we describe a variation in an electronic phase with x of $Eu_{1-x}Sr_xMnO_3$ ($0.3<x<0.7$) single crystals that show the FM with the lowest T_C (~40 K) due to the narrowest W. In the vicinity of $x=0.5$, neither a FM or the CO/OO ($q=1/2$) is formed in a long range due to both of the narrowed W and increased quenched disorder. Another noteworthy aspect is that the CO/OO ($q\sim1/3$) appears at $x>0.5$, being analogous to $La_{1-x}Ca_xMnO_3$ ($x\sim0.66$) (Refs. 26–28) and $Sm_{1-x}Sr_xMnO_3$ ($x>0.5$).[29] In $Eu_{1-x}Sr_xMnO_3$, therefore, in addition to the competition between the FM and the $q=1/2$ CO/OO in a short range at $x\sim0.5$, another competition is seen between the $q\sim1/3$ CO/OO and the A-type antiferromagnetic (AF) phase at $x>0.5$. In following, we first describe experimental procedures in Sec. II. In Sec. III, we describe an overview of the electronic phase diagram (Sec. III A), competing features in the vicinity of $x=0.5$ (Sec. III B), metal-insulator phenomena induced by an external magnetic field (Sec. III C), and an appearance of the $q\sim1/3$ CO/OO at $x>0.5$ (Sec. III D). Summary is given in Sec. IV.

II. EXPERIMENTAL PROCEDURES

Single crystals of $Eu_{1-x}Sr_xMnO_3$ have been prepared by the floating zone method. The mixtures of Eu_2O_3, $SrCO_3$, and Mn_2O_3 powders with a prescribed ratio were calcined at 1050 °C in air for 12–24 h. The mixtures were then pulverized and pressed into a rod with about 50 mm in length and 4 mm in diameter. The rod was then sintered at 1300–1350 °C in air for 12 h.

TABLE I. The analyzed cation ratio, lattice parameters, and transition temperatures of $Eu_{1-x}Sr_xMnO_3$ (x=0.45, 0.5, and 0.55) prepared by the floating zone method.

x (nominal)	x Sr/(Eu+Sr) [a]	Lattice parameters, a_0, b_0, and c_0 (Å)	T_C,[b] T_G,[c] and T_N [b] (K)
0.45	0.465	a_0=5.4281, b_0=5.4260, c_0=7.6493	62.0[b]
0.5	0.507	a_0=5.4331, b_0=5.4171, c_0=7.6367	43.8[c]
0.55	0.562	a_0=5.4441, b_0=5.4149, c_0=7.6076	158.6[b]

[a] The cation ratio has been determined by the ICP spectroscopy.

[b] The averaged value determined from the resistivity in the cooling and warming runs.

[c] The temperature at which the ZFC magnetization at 0.5 T becomes maximum.

The crystal growth of $Eu_{1-x}Sr_xMnO_3$ was performed with oxygen gas flowing by using the floating zone furnace equipped with the double hemiellipsoidal mirrors coated with gold. Two halogen incandescent lamps were used as heat sources. During the crystal growth, the upper and lower rods were rotated in opposite directions and the growth rate was set at 15–25 mm/h. The obtained melt-grown crystal was pulverized and checked by an x-ray powder diffraction (XRD) with Cu $K\alpha$ radiation (MXP18 AHF,[22] MAC Science Co., Ltd). The diffraction pattern was collected by the $\theta/2\theta$ step scanning method with ranging $15° \leq 2\theta \leq 110°$. Rietveld refinement of the XRD pattern indicated that the obtained crystal is of single phase. The crystals for $x \leq 0.59$ are orthorhombic *Pbnm* ($a_0 \sim b_0 \sim c_0/\sqrt{2} \sim \sqrt{2}a_p$, where a_p is an axis of the pseudocubic lattice) while those for $x \geq 0.6$ tetragonal $I4/mcm$.[30,31] The crystals are in single domains in a sense of the pseudocubic lattice but in multidomains in lower symmetries. The cation ratio of the obtained crystals was also checked by the inductively coupled plasma (ICP) spectroscopy. The analyzed cation ratio, lattice parameters, and the transition temperatures for several crystals of $Eu_{1-x}Sr_xMnO_3$ are listed in Table I.

The magnetization up to 7 T was measured by a superconducting quantum interference device magnetometer (Magnetic Property Measurement System (MPMS), Quantum Design Inc.). After the crystal was cooled down to the lowest temperature in zero field, the magnetic field was applied, and the zero-field-cooled (ZFC) magnetization was measured with increasing temperature. The field-cooled (FC) magnetization was subsequently measured with decreasing temperature in a same magnetic field. Resistivity in magnetic fields was measured in a cryostat equipped with a superconducting magnet with the magnetic field parallel to the transport current. For these measurements in magnetic fields, no attention has been paid for the relative angle between the direction of the magnetic field and the pseudocubic axis of the crystals. A single-crystal x-ray diffraction was performed using an imaging plate system monochromated with Mo $K\alpha$ radiation. A crystal was mounted on a goniometer with a (1 0 0) plane of the pseudocubic setting almost parallel to a beam axis. The temperature was changed down to ~50 K with use of a closed cycle helium refrigerator.

For a crystal of $Eu_{1-x}Sr_xMnO_3$ (x=0.47), the x-ray diffraction measurement was performed at the beam line BL-1A, photon factory, KEK (High Energy Accelerator Research Organization) with use of the imaging plate system equipped with the Si-double-crystal monochromatized synchrotron radiation (λ=0.6878 Å). The crystal was attached on a glass fiber and the temperature was changed flowing helium gas.

III. RESULTS AND DISCUSSION

A. An overview of the electronic phase diagram

Figure 1 shows a variation in the electronic phase with x of $Eu_{1-x}Sr_xMnO_3$ ($0.3 < x < 0.7$) single crystals. In Fig. 1, a FM appears at $0.38 \leq x < 0.47$; the transition is strongly of first order, accompanying the hysteresis (open and closed squares in Fig. 1). The critical temperature (T_C) reaches the mximum at $x \sim 0.43$ but is still the lowest among the FM of the perovskite manganites. In the vicinity of x=0.5 ($0.48 \leq x \leq 0.5$), a SGI appears. As x further increases, similarly to the cases of $RE_{1-x}Sr_xMnO_3$ (RE=La, Pr, Nd, and Sm), the

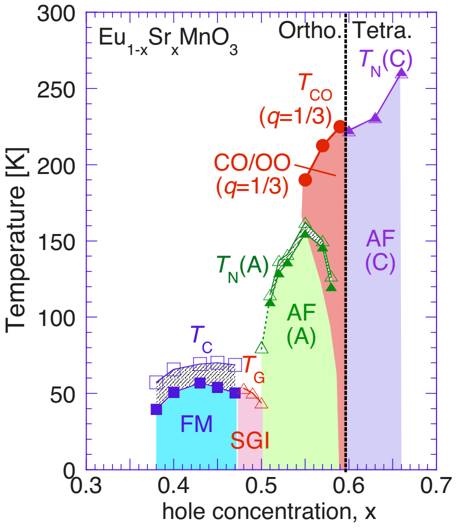

FIG. 1. (Color online) The electronic phase diagram of $Eu_{1-x}Sr_xMnO_3$ ($0.35 < x < 0.7$) single crystals. The ferromagnetic metal, the spin-glasslike insulator, the A-type antiferromagnetic state, the charge/orbital ordering ($q=1/3$), and the C-type antiferromagnetic states are denoted as FM, SGI, AF(A), CO/OO ($q=1/3$) and AF(C), respectively. T_C, T_G, T_N(A), T_{CO}($q=1/3$), and T_N(C) are the transition temperatures from (to) the respective phases denoted as open (closed) diamonds, squares, red triangles, green triangles, red circles, and violet triangles, respectively. The boundaries between an orthorhombic phase and a tetragonal phase are denoted as dotted lines.

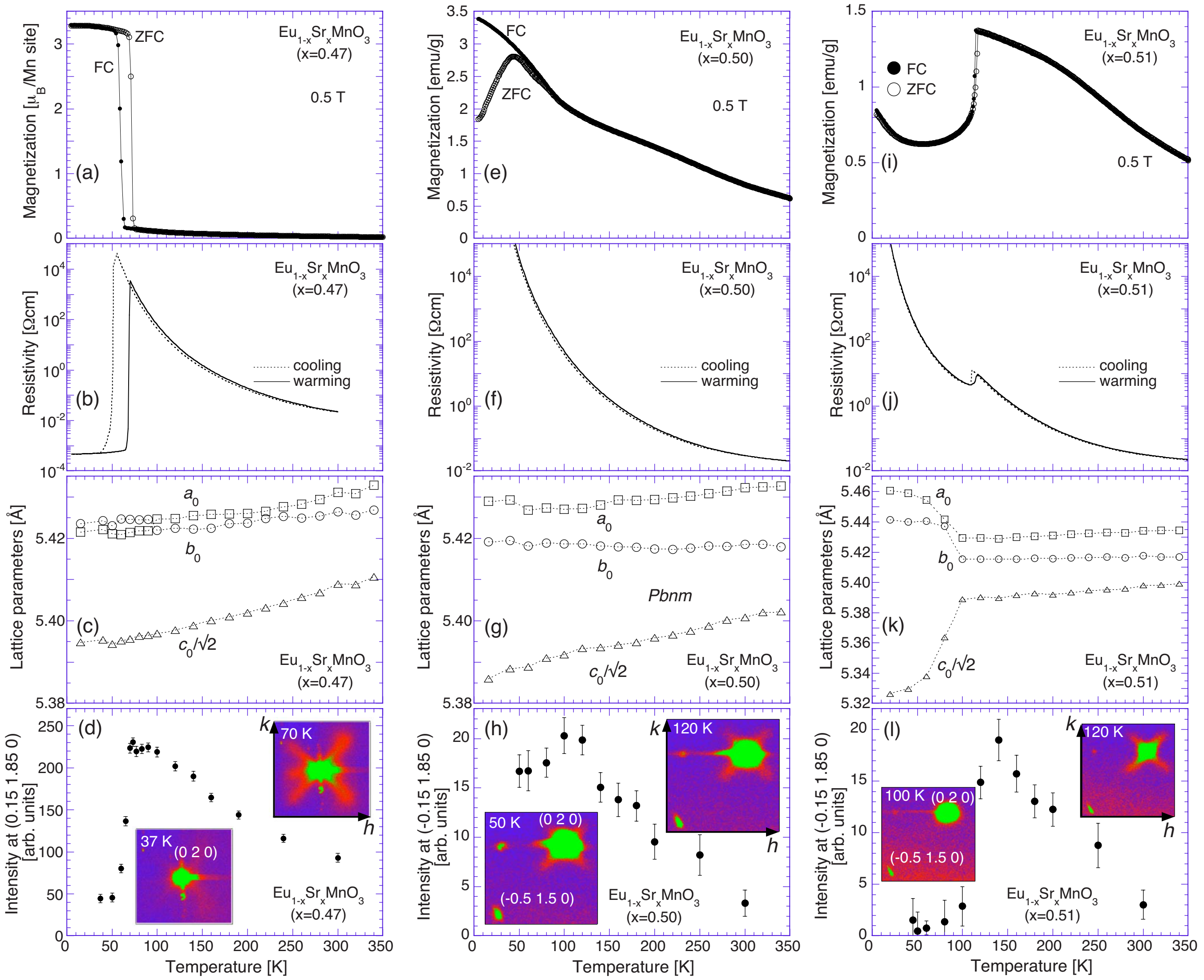

FIG. 2. (Color online) Temperature profiles of [(a), (e), and (i)] magnetization, [(b), (f), and (j)] resistivity, [(c), (g), and (k)] lattice parameters, and [(d), (h), and (l)] an intensity of an x-ray diffuse scattering at (0.15 1.85 0), or (−0.15 1.85 0) of the pseudocubic setting for the crystals of [(a)–(d)] $x=0.47$, [(e)–(h)] 0.5, and [(i)–(l)] 0.51, respectively. Insets (left, right) are single-crystal x-ray diffuse scatterings at (37 K, 70 K), (50 K, 120 K), and (100 K, 120 K) for (d) $x=0.47$, (h) 0.5, and (l) 0.51, respectively. Reflections locating near (0 2 0) in the insets of (h) and (l) are due to the twinning of the crystals.

A-type and the C-type AF phases appear at $0.5<x<0.6$ and $0.6\leq x$, respectively. The A-type AF phase becomes optimal at $x\sim0.55$, the critical temperature of which [T_N(A)] is about 160 K. The T_N for the C-type AF phase is about 220 K at $x=0.6$ and increases as x increases beyond 0.6.

In an orthorhombic region of $0.55\leq x\leq0.59$ in Fig. 1, the charge/orbital ordering with $q\sim1/3$ appears above the A-type AF phase.[29] Although a critical temperature for the CO/OO ($q\sim1/3$) [$T_{CO}(q=1/3)$] shows increasing as x increases from 0.55 to 0.59, the CO/OO ($q\sim1/3$) together with the lower-lying A-type AF phase at $x<0.6$ are abruptly replaced with C-type AF phase for $x\geq0.6$, where a crystal structure changes from orthorhombic to tetragonal $I4/mcm$.

B. Competing features in the vicinity of $x=0.5$

Figure 2 shows temperature profiles of [(a), (e), and (i)] magnetization, [(b), (f), and (j)] resistivity, [(c), (g), and (k)] lattice parameters, and [(d), (h), and (l)] x-ray diffuse scattering for the crystals of [(a)–(d)] $x=0.47$, [(e)–(h)] 0.5, and [(i)–(l)] 0.51, respectively. The charge or orbital correlation ($q=1/2$) in a short range is quantified by an x-ray diffuse scattering around (0 2 0) of a pseudocubic setting.[32] In Figs. 2(d), 2(h), and 2(l), the intensity at (0.15 1.85 0) [or (−0.15 1.85 0)] was estimated by fitting the profile of ($0.15+\delta/2$ $1.85+\delta/2$ 0) [or ($-0.15-\delta/2$ $1.85+\delta/2$ 0)] ($-0.5\leq\delta\leq0.5$) with a Gaussian form. In Figs. 2(a) and 2(b) are seen a jump (drop) in FC (ZFC) magnetization and a steep decrease (increase) in resistivity in the cooling (warming) run at about 50 K (70 K), respectively. In Fig. 2(c), the c_0 continues to decrease with decrease in temperature but it becomes almost unchanged below 50 K. Figures 2(a)–2(c) are indicative of the FM ground state. In Figs. 2(i) and 2(j) are seen a decrease (increase) in magnetization and a decrease

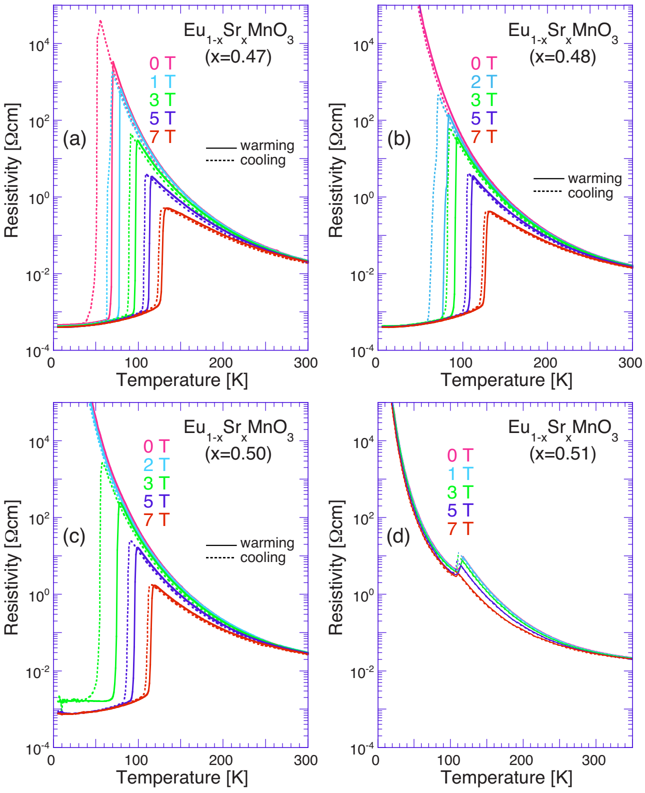

FIG. 3. (Color online) Temperature profiles of resistivity in magnetic fields for the $Eu_{1-x}Sr_xMnO_3$ crystals with (a) $x=0.47$, (b) 0.48, (c) 0.5, and (d) 0.51, respectively. The cooling and warming runs are denoted with dotted and solid lines, respectively.

(increase) in resistivity in a cooling (warming) run at about 115 K, respectively. In Fig. 2(k), shrinkage of c_0 and elongations of a_0 as well as b_0 are observed at around 100 K. These results are indicative of the A-type AF phase. In accord, the intensities of the x-ray diffuse scattering decrease upon the respective transitions [Figs. 2(d) and 2(l)]. Figures 2(a)–2(d) and 2(i)–2(l) indicate, therefore, that short-range charge/orbital ordering ($q=1/2$) is removed upon appearance of the FM and the A-type AF phase in a long range for $x=0.47$ and 0.51, respectively.[14]

In Fig. 2(e) for $x=0.5$, however, discrepancy between ZFC and FC magnetizations is observed to be conspicuous below about 50 K, which is typical for a spin-glass state. As shown in Fig. 2(f), resistivity remains insulating down to the lowest temperature. The intensity of an x-ray diffuse scattering [Fig. 2(h)] increases as temperature decreases down to 100 K. Then, it turns into decreasing below 100 K but remains finite at the lowest temperature. Figures 2(e)–2(h) indicate that for $x=0.5$ a SGI is realized with a finite intensity of the CO/OO ($q=1/2$) in a short range. In $Eu_{1-x}Sr_xMnO_3$, therefore, the CO/OO ($q=1/2$) cannot be formed in a long-range manner due to an increased quenched disorder upon alloying of Eu/Sr.

C. Metal-insulator phenomena induced by an external magnetic field

In Fig. 3 are shown temperature profiles of resistivity in magnetic fields for the crystals of (a) $x=0.47$, (b) 0.48, (c) 0.5, and (d) 0.51, respectively. In Fig. 3(a), the critical temperature for the nonmetal to metal transition remarkably increases from about 50 K at zero field to about 120 K at 7 T in the cooling run. As seen in Figs. 3(b) and 3(c), spin-glasslike insulators are kept at low magnetic fields while the ferromagnetic metals appear at $\mu_0 H \geq 2$ and 3 T for $x=0.48$ and 0.5, respectively. The A-type AF state survives at low temperatures even at 7 T [Fig. 3(d)], although negative magnetoresistance is seen above T_N(A) due to field-enhanced ferromagnetic correlation.

Figure 4 shows magnetization (upper panels) and resistivity (lower panels) isotherms for the crystals of $x=0.47$ (left), 0.48 (middle), and 0.5 (right), respectively. The versions at lower temperatures are indicated for $x=0.48$ and 0.5 in Fig. 5. In these figures, large changes in resistivity are accompanied by metamagnetic transitions. In Fig. 4 (left), the critical magnetic field to induce the transition at 110 K is about 5 T while that at 60 K, just above T_C, is lowered to about 0.4 T. Similar features are seen in Fig. 4 (middle) and Fig. 4 (right), as temperature is lowered down to 50 K. With further decrease in temperature, however, as indicated in Fig. 5, an increase in the critical field and hysteretic or irreversible features are pronounced due to the nature of the first-order phase transition.

Figure 6 shows the electronic phase diagrams in the vicinity of $x=0.5$ plotted on the temperature vs magnetic field plane which are composed of the FM, SGI, and the A-type AF nonmetal for the $x=0.47$, 0.48, 0.49, 50, and 0.51 crystals. It is demonstrated in this figure that for $x=0.48\sim 0.5$, the SGI at zero field is altered to the FM by application of an external magnetic field. For $x=0.51$, however, the A-type AF nonmetal is so stable that the FM does not appear for $\mu_0 H < 7$ T.

D. A-type antiferromagnetic state and charge/orbital ordering ($q\sim 1/3$) at $x>0.5$

In Fig. 7 are shown temperature profiles of [(a), (e), and (i)] magnetization, [(b), (f), and (j)] resistivity, [(c), (g), and (k)] lattice parameters, and [(d), (h), and (l)] an intensity of a superlattice (SL) for the crystals of [(a)–(d)] $x=0.55$, [(e)–(h)] 0.57, and [(i)–(l)] 0.59, respectively. In Fig. 7(d), an intensity of diffuse scattering is also indicated. Decreases in both magnetization and resistivity are seen at about 155 K in Figs. 7(a) and 7(b), respectively. At this temperature, shrinkage of c axis as well as elongations of a and b axes is observed [Fig. 7(c)]. These results shown in Figs. 7(a)–7(c) thus indicate that the $x=0.55$ crystal undergoes the transition to the A-type AF phase accompanied by the x^2-y^2 orbital ordering below about 155 K. In Fig. 7(d), as shown in the inset (right), a diffuse scattering around (0 2 0) is visible at 200 K. As temperature decreases, however, the diffuse scattering changes to a SL spot, the position of which is not at the midpoint between ($-1/2$ 3/2 0) and (0 2 0) but closer to (0 2 0), i.e., ($-\varepsilon/2$ $2-\varepsilon/2$ 0) with $\varepsilon\sim 1/3$ as shown in the inset (left).[29] In Fig. 7(d), the intensity of the SL spot first increases with decrease in temperature but steeply decreases below 160 K. As temperature further decreases, the SL spot seems to disappear below 100 K.

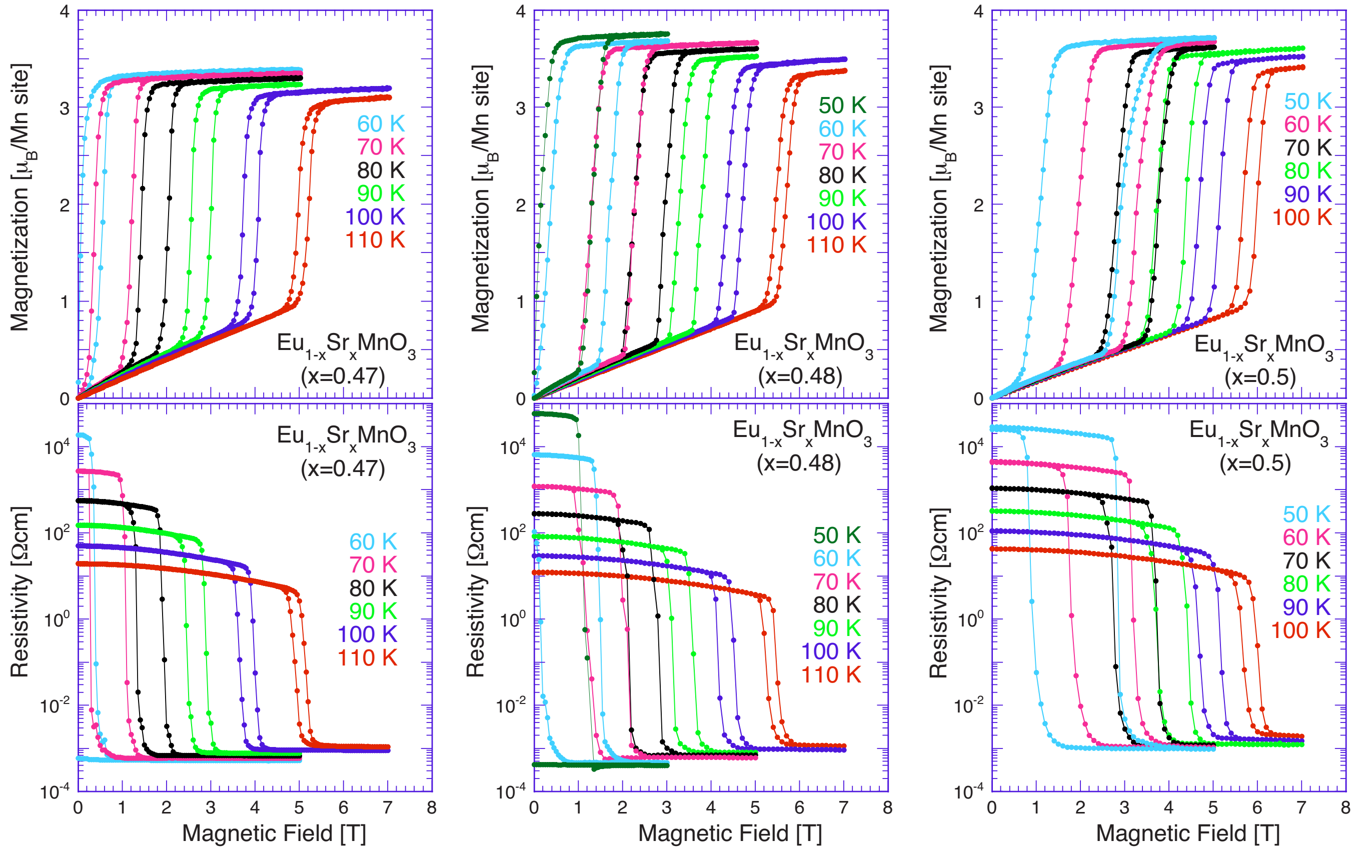

FIG. 4. (Color online) The magnetization (upper panels) and resistivity (lower panels) isotherms for the $\mathrm{Eu}_{1-x}\mathrm{Sr}_x\mathrm{MnO}_3$ crystal with $x=0.47$ (left), 0.48 (middle), and 0.5 (right), respectively.

In Figs. 7(e)–7(g) for $x=0.57$, changes in magnetization, resistivity, and lattice parameters, similar to those in Figs. 7(a)–7(c), are seen around 155 K, which are indicative of the A-type AF phase. The respective changes in the physical quantities upon the transition in Figs. 7(e)–7(g) are, however, more broadened than those in Figs. 7(a)–7(c). In Fig. 7(h), a weak but discernable SL spot is seen even at 225 K, as shown in the inset (right). As temperature decreases, the intensity of the spot increases at first. Below 160 K, however, it turns into decreasing and disappears below about 50 K, similarly to the case of $x=0.55$ shown in Fig. 7(d).

The $x=0.59$ crystal locates in the vicinity of the boundary between an orthorhombic phase and a tetragonal phase in Fig. 1, where the CO/OO ($q\sim1/3$) is more distinctly seen. In Fig. 7(i), a peak of magnetization is seen at ∼255 K. Figure 7(j) shows correspondingly a subtle change in a slope of resistivity ($d\rho/dT$) at about 225 K. (An anomaly in resistivity around 100 K is due to appearance of the A-type antiferromagnetic phase.) In Fig. 7(l), similarly to the cases of the $x=0.55$ and 0.57 crystals, a SL spot at ($\varepsilon/2\ 2-\varepsilon/2\ 0$) with $\varepsilon\sim1/3$ appears below about 225 K, as shown in the inset (right). Being distinct from $x=0.55$ and 0.57 crystals, the intensity of the spot keeps increasing down to the lowest temperature, as shown in the inset (left). For $x=0.59$ with the hole concentration nearest to 2/3, the CO/OO ($q\sim1/3$) should be more stabilized than that for $x=0.55$ and 0.57, which may lead to the coexistence of the CO/OO ($q\sim1/3$) and A-type AF phases.

For the temperature dependence of the modulation of the $q\sim1/3$ CO/OO, Fig. 8 indicates temperature evolutions of the x-ray diffraction profiles ranging from (0 2 0) to ($\pm1/2$ 3/2 0), i.e., ($\pm\Delta h/2\ 2-\Delta h/2\ 0$) with $-0.5\leq\Delta h\leq1.5$, for the crystals of $x=0.55$ (left), 0.57 (middle), and 0.59 (right). In all the cases the SLs at $\Delta h\sim0.3$–0.4 become visible as temperature decreases; the intensities of the SLs for $x=0.55$ and 0.57 become maximum at 160 K [Figs. 8 (left) and 8 (middle)]. Figure 8 (right) clearly indicates that the SL remains finite even at the lowest temperature (50 K) for $x=0.59$. It is also seen in Fig. 8 (right) that as temperature decreases the peak position of the SL moves toward higher Δh. That is, the position is almost commensurate at $\Delta h\sim1/3$ at 225 K while it incommensurate at $\Delta h\sim0.42$ at 50 K. Such a temperature dependent crossover from commensurate to incommensurate is quite analogous to the charge ordering in $\mathrm{La}_{2-x}\mathrm{Sr}_x\mathrm{NiO}_4$ with x around 1/3.[33] A mixing in nanoscale of the $q=1/2$ and 1/3 CO/OO below T_{CO} ($q=1/3$) might also cause an apparent crossover from commensurate to incommensurate.[34] However, both electron and x-ray diffraction patterns show no indication that two SLs appear simultaneously at commensurate positions of ($\pm\varepsilon/2\ 2-\varepsilon/2\ 0$) with $\varepsilon=1/2$ and 1/3. The coexistence of the $q=1/2$ and 1/3 CO/OO might happen but it might not be so stable as the bulk property.

IV. SUMMARY

The x-dependent electronic state in $\mathrm{Eu}_{1-x}\mathrm{Sr}_x\mathrm{MnO}_3$ ($0.35<x<0.7$) single crystals have been investigated, which un-

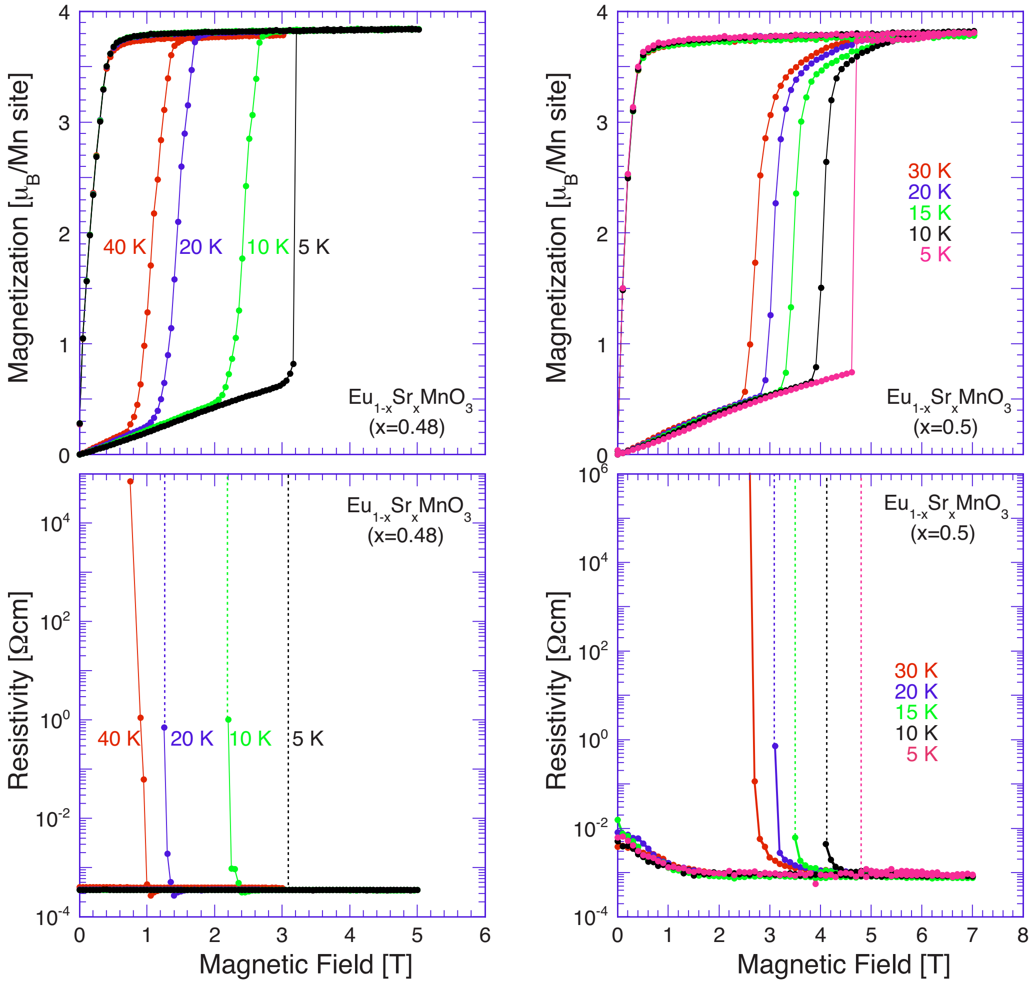

FIG. 5. (Color online) The magnetization (upper panels) and resistivity (lower panels) isotherms below 50 K for the crystals of $x=0.48$ (right) and 0.5 (left), respectively.

dergoes the phase change such as the ferromagnetic metal ($0.38 \leq x \leq 0.47$), a spin-glasslike insulator in the vicinity of $x=0.5$ ($0.48 \leq x \leq 0.5$), the A-type ($0.51 \leq x < 0.6$) and C-type ($0.6 \leq x$) antiferromagnetic state. The T_C for the ferromagnetic transition is steeply suppressed below about 60 K compared with the other perovskite manganites.

Due to both of a narrowed one-electron bandwidth of the e_g band and increased disorder upon the alloying of Eu/Sr, the charge/orbital ordering ($q=1/2$) cannot be formed in a long-range manner even in the vicinity of $x=0.5$. Instead, a spin-glasslike insulator appears in which the charge/orbital ordering ($q=1/2$) in a short range exists. However, such a charge/orbital ordering disappears upon the formation of the ferromagnetic metal ($x \leq 0.47$) or the A-type antiferromagnetic state ($x \geq 0.51$). At $x \sim 0.5$, an application of an external magnetic field also removes the short-range charge/orbital ordering ($q=1/2$), which leads to an insulator-metal transition or colossal magnetoresistance behavior.

In a broad range of x ($0.55 \leq x \leq 0.59$), at temperatures above the A-type antiferromagnetic phase, the charge/orbital ordering appears with the modulation vector (0, q, 0) with $q \sim 1/3$ in the orthorhombic *Pbnm* setting ($a_0 \sim b_0 \sim c_0/\sqrt{2} \sim \sqrt{2}a_p$, a_p being the lattice parameter of the pseudocubic lattice). In $Eu_{1-x}Sr_xMnO_3$, the critical temperature for the

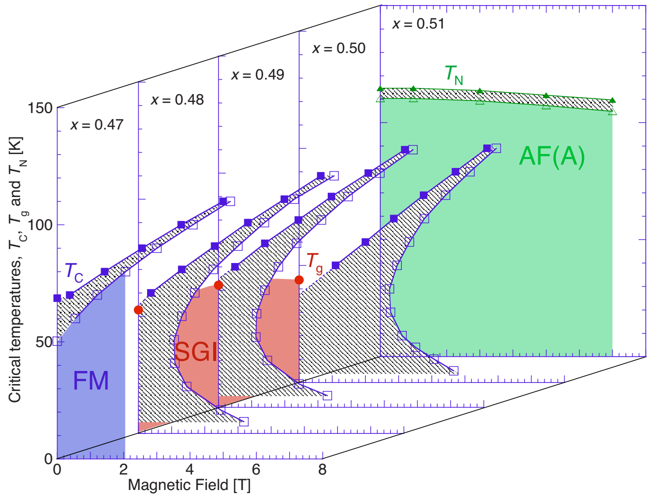

FIG. 6. (Color online) The phase diagrams among the FM, SGI, and A-type antiferromagnetic state [AF(A)] for $Eu_{1-x}Sr_xMnO_3$ crystals with $x=0.47$, 0.48, 0.49, 0.5, and 0.51 as plotted on the temperature vs magnetic field plane. The transitions from (to) the FM and AF(A) are denoted as open (solid) squares and triangles, respectively. The transition temperatures for the SGI are denoted with closed circles. The hysteresis regions are hatched.

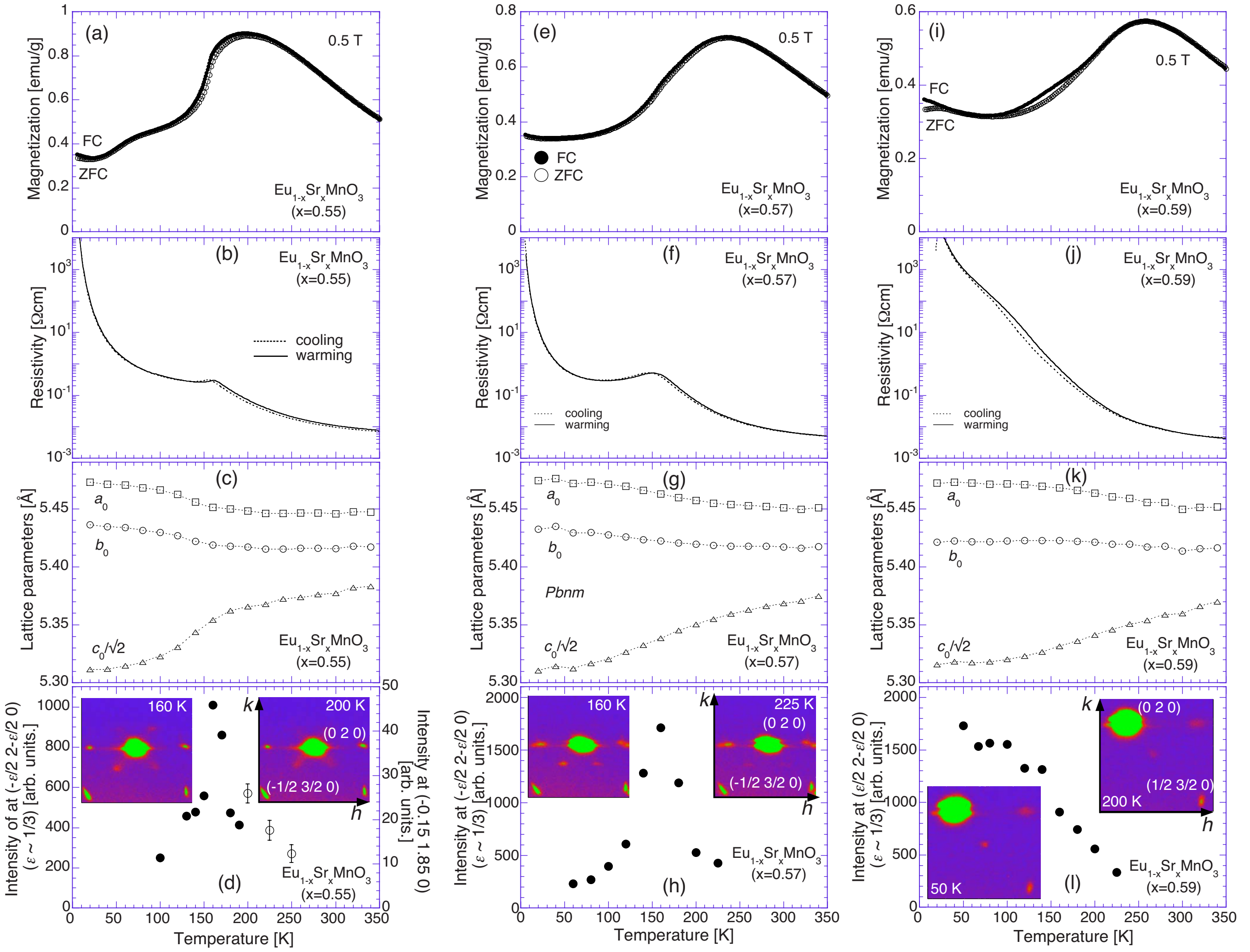

FIG. 7. (Color online) Temperature profiles of [(a), (e), and (i)] magnetization, [(b), (f), and (j)] resistivity, [(c), (g), and (k)] lattice parameters, and [(d), (h), and (l)] an intensity of a superlattice at $(\pm\varepsilon/2\ 2-\varepsilon/2\ 0)$ with $\varepsilon\sim 1/3$ of the pseudocubic setting for the crystals of [(a)–(d)] $x=0.55$, [(e)–(h)] 0.57, and [(i)–(l)] 0.59, respectively. In (d), an intensity of an x-ray diffuse scattering at (0.15 1.85 0) is also indicated. Insets (left, right) are single-crystal x-ray diffraction patterns at (160 K, 200 K), (160 K, 225 K), and (50 K, 200 K) for (d) $x=0.55$, (h) 0.57, and (l) 0.59, respectively. Reflections near (0 2 0) are due to twinnings of the crystals.

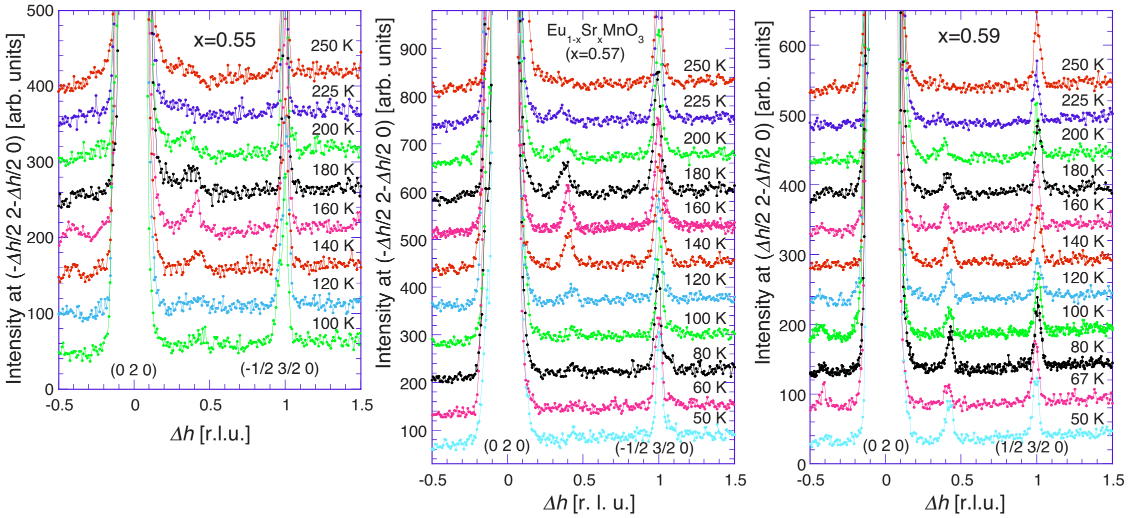

FIG. 8. (Color online) Temperature evolutions of the x-ray diffraction profiles ranging from (0 2 0) to $(\pm 1/2\ 3/2\ 0)$ [see also Figs. 7(d)–7(l)], i.e., $(\pm\Delta h/2\ 2-\Delta h/2\ 0)$ with $-0.5\leq\Delta h\leq 1.5$, for the crystals of $x=0.55$ (left), 0.57 (middle), and 0.59 (right).

A-type antiferromagnetic state is so lowered due to the narrowed one-electron bandwidth that the charge/orbital ordering ($q \sim 1/3$) becomes alternatively visible. The modulation of the charge/orbital ordering is temperature dependent; $q \sim 1/3$ upon the transition while $q > 1/3$ at low temperatures.

ACKNOWLEDGMENTS

The authors would like to thank X. Z. Yu and Y. Matsui in Advanced Nano Characterization Center (ANCC), National Institute for Materials Science (NIMS) for the helpful discussions.

---

[1] Y. Tokura and N. Nagaosa, Science **288**, 462 (2000).
[2] E. Dagotto, T. Hotta, and A. Moreo, Phys. Rep. **344**, 1 (2001).
[3] Y. Tokura, Rep. Prog. Phys. **69**, 797 (2006).
[4] G. H. Jonker and J. H. van Santen, Physica (Amsterdam) **16**, 337 (1950).
[5] G. H. Jonker, Physica (Amsterdam) **22**, 707 (1956).
[6] C. Zener, Phys. Rev. **82**, 403 (1951).
[7] P. W. Anderson and H. Hasegawa, Phys. Rev. **100**, 675 (1955).
[8] P.-G. de Gennes, Phys. Rev. **118**, 141 (1960).
[9] N. Furukawa, J. Phys. Soc. Jpn. **64**, 2754 (1995).
[10] J. B. Torrance, P. Lacorre, A. I. Nazzal, E. J. Ansaldo, and Ch. Niedermayer, Phys. Rev. B **45**, 8209 (1992).
[11] Y. Tokura, A. Urushibara, Y. Moritomo, T. Arima, A. Asamitsu, G. Kido, and N. Furukawa, J. Phys. Soc. Jpn. **63**, 3931 (1994).
[12] A. Urushibara, Y. Moritomo, T. Arima, A. Asamitsu, G. Kido, and Y. Tokura, Phys. Rev. B **51**, 14103 (1995).
[13] H. Kuwahara, Y. Tomioka, A. Asamitsu, Y. Moritomo, and Y. Tokura, Science **270**, 961 (1995).
[14] Y. Tomioka, H. Hiraka, Y. Endoh, and Y. Tokura, Phys. Rev. B **74**, 104420 (2006).
[15] G. C. Milward, M. J. Calderon, and P. B. Littlewood, Nature (London) **433**, 607 (2005).
[16] L. M. Rodriguez-Martinez and J. P. Attfield, Phys. Rev. B **54**, R15622 (1996).
[17] A. Maignan, C. Martin, G. VanTendeloo, M. Hervieu, and B. Raveau, Phys. Rev. B **60**, 15214 (1999).
[18] L. M. Rodriguez-Martinez and J. P. Attfield, Phys. Rev. B **63**, 024424 (2000).
[19] T. Terai, T. Sakaki, T. Kakeshita, T. Fukuda, T. Saburi, H. Kitagawa, K. Kindo, and M. Honda, Phys. Rev. B **61**, 3488 (2000).
[20] A. Sundaresan, A. Maignan, and B. Raveau, Phys. Rev. B **55**, 5596 (1997).
[21] S. Nakamura, S. Shimomura, N. Ikeda, S. Nimori, T. Takeuchi, and K. Itoh, J. Phys. Soc. Jpn. **73**, 3059 (2004).
[22] I. O. Troyanchuk, N. V. Samsonenko, N. V. Kasper, H. Szymczak and A. Nabialek, Phys. Status Solidi A **160**, 195 (1997).
[23] Y. M. Mukovskii, G. Hilscher, H. Michor, and A. M. Ionov, J. Appl. Phys. **83**, 7163 (1998).
[24] Y. Tadokoro, Y. J. Shan, T. Nakamura, and S. Nakamura, Solid State Ionics **108**, 261 (1998).
[25] S. Nakamura, Y. Tadokoro, Y. J. Shan, and T. Nakamura, J. Phys. Soc. Jpn. **68**, 1485 (1999).
[26] C. H. Chen, S.-W. Cheong, and H. Y. Hwang, J. Appl. Phys. **81**, 4326 (1997).
[27] S. Mori, C. H. Chen, and S.-W. Cheong, Nature (London) **392**, 473 (1998).
[28] P. G. Radaelli, D. E. Cox, L. Capogna, S.-W. Cheong, and M. Marezio, Phys. Rev. B **59**, 14440 (1999).
[29] Y. Tomioka, X. Z. Yu, T. Ito, Y. Matsui, and Y. Tokura, Phys. Rev. B **80**, 094406 (2009).
[30] A. Sundaresan, V. Caignaert, B. Raveau, and E. Suard, Solid State Commun. **104**, 489 (1997).
[31] F. Damay, C. Martin, M. Hervieu, A. Maignan, B. Raveau, G. Andre, and F. Boure, J. Magn. Magn. Mater. **184**, 71 (1998).
[32] S. Shimomura, N. Wakabayashi, H. Kuwahara, and Y. Tokura, Phys. Rev. Lett. **83**, 4389 (1999).
[33] K. Ishizaka, T. Arima, Y. Murakami, R. Kajimoto, H. Yoshizawa, N. Nagaosa, and Y. Tokura, Phys. Rev. Lett. **92**, 196404 (2004).
[34] X. Z. Yu, Y. Tomioka, T. Asaka, K. Kimoto, T. Arima, Y. Tokura, and Y. Matsui, Appl. Phys. Lett. **94**, 082509 (2009).